Results in Physics 24 (2021) 104041

Contents lists available at ScienceDirect

Results in Physics

journal homepage: www.elsevier.com/locate/rinp

Finite amplitude electron-acoustic waves in the electron diffusion region

Odutayo R. Rufai [a,*], George V. Khazanov [a], S.V. Singh [b]

[a] Heliophysics Division, NASA Goddard Space Flight Center, Greenbelt, MD, USA
[b] Indian Institute of Geomagnetism, New Panvel (W), Navi Mumbai 410218, India

ARTICLE INFO

Keywords:
MMS observations
Kinetic vortex-like velocity distribution
Adiabatic fluid
Electron-acoustic waves
Reductive perturbation technique
Aymmetric ESWs
Electron diffusion region (EDR)
Earth's magnetopause

ABSTRACT

The electron-acoustic solitons are studied with two temperature electrons (a hot trapped having vortex-like velocity distribution and a warm adiabatic fluid) and stationary ions. The theoretical model is based on the observations of a mixture of the hot, tenuous magnetospheric and warm, dense magnetosheath plasma particles associated with the asymmetric magnetic reconnection at the Earth's magnetopause by Magnetospheric Multiscale (MMS). Using the reductive perturbation technique, the model supports the existence of nonlinear electron-acoustic structures derived from the mKdV-like equation. The electron-acoustic waves propagate at supersonic speeds above the electron sound speed. The results are applied to observations of electric field structures in the electron diffusion region (EDR).

Introduction

Spacecraft missions such as Cluster [1,2], THEMIS [3,4], and Magnetospheric Multiscale (MMS) [5] observations revealed that plasma wave and turbulence such as broadband electrostatic noise can be generated during the magnetic reconnection process in the Earth's magnetosphere. Such fluctuations and turbulence are observed in all parts of the reconnection region, such as separatrix regions [6], outflows [7], and ion and electron diffusion region [8,9]. At the Earth's magnetopause, magnetic reconnection process occurs in an asymmetric system between warm, dense plasmas in the magnetosheath and low-density plasmas in the magnetosphere, which contains tenuous, hot plasma as well as a cold plasma populations [9–14]. MMS mission also observed symmetric electric field structures in the Earth's magnetotail [15,16]. As the magnetic field lines break and reconnect, the energy dissipates and diffuses at small and large scales in the diffusion regions. The ion species are found demagnetized inside both ion diffusion region (IDR) and electron diffusion region (EDR), whereas electrons are only demagnetized inside the EDR [11].

Through the MMS mission, the electron plasma heating and acceleration in the EDR has been revealed, particularly at the Earth's magnetopause where asymmetric electric field structures were observed [5]. On 11 July 2017, MMS traversed the magnetotail current sheet, observing tailward-to-earthward outflow reversal, current-carrying electron jets in the direction along the electron meandering motion or out-of-plane direction, agyrotropic electron distribution functions, and dissipation signatures [17]. Later reports confirmed that the electrons penetrating into the diffusion region of the Earth's magnetopause exhibit meandering motion that produced electron agyrotropy, that is, crescent-shaped electron distribution [16,18,19]. Numerous theories and simulation of EDR events [11,20–23] suggested that crescent structures are formed by finite gyroradius effects of accelerated magnetosheath particles merging with the inflowing magnetosphere plasma. Hwang et al.[16] reported MMS observations of enhanced electron vorticity during the magnetic reconnection in the vicinity of the electron diffusion region (EDR). Recent MMS spacecraft observations in the electron diffusion region of the Earth's magnetosphere have recorded small [24] and large [9,25] amplitude electric field fluctuations. Mozer et al. [26] reported the MMS observations of large amplitude bipolar electric field structures at the Earth's magnetopause with trapped electron species inside the electron phase space holes of time domain structures (TDS) or electrostatic solitary waves (ESWs). On the other hand, in the Earth's magnetotail MMS observations revealed a super-slow ESWs with small amplitude bipolar electric field [27]. These electric field structures can be identified with the general characteristics of electrostatic solitary waves (ESWs) [29], usually monopolar, bipolar, or tripolar pulses which can have either positive or negative, or both negative and positive polarities. Fig. 1 (Fig. 1 (l) of Ergun et al. [9]) show an example of a sequence of asymmetric electric field (E_z) structures parallel to the magnetic field observed by MMS satellite for 10s on 22 October 2015 during magnetic reconnection at the Earth's magnetopause. It is seen that the maximum amplitude of the parallel electric field

* Corresponding author.
E-mail address: odutayoraji.rufai@nasa.gov (O.R. Rufai).

https://doi.org/10.1016/j.rinp.2021.104041
Received 8 January 2021; Received in revised form 1 March 2021; Accepted 3 March 2021
Available online 23 March 2021

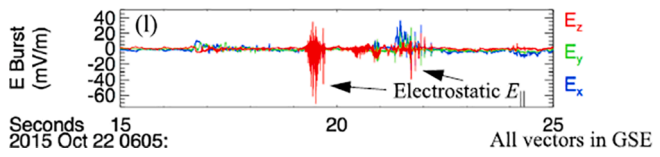

Fig. 1. Example of parallel electric field structures (E_z in red) in z-direction observed by MMS during the magnetic reconnection at the magnetopause [9]. (For interpretation of the references to colour in this figure legend, the reader is referred to the web version of this article.)

fluctuations is less than 40 mV/M [9].

Several types of waves have been involved in electron diffusion region, which include electrostatic solitary waves [10,25] and other instabilities. The electrostatic solitary waves (ESWs) or Time domain structures (TDS)[28] observed in different regions of the Earth's magnetosphere have been identified with both symmetric and asymmetric bipolar parallel electric field (magnetic field-aligned) structures. The ESWs associated with symmetric bipolar parallel electric field structures are electron phase holes and there are divergent kinetic Bernstein-Greene-Kruskal (BGK) models [30,31]. Whereas asymmetric bipolar parallel electric field structures of ESWs which can be explained using nonlinear fluid dynamic theory, expected to have convergent electric field configuration for the existence of electron-acoustic solitons and double layers [32–34]. However, the relationship between the amplitude and the width of the two major types of ESWs is of great importance from the theoretical point of view. The kinetic BGK theoretical analysis has shown that the amplitude increases with increasing in width [26], for symmetric electron phase holes TDS/ESWs. For the asymmetric ESWs (solitons), the wave amplitude increases with a decrease in width. The small but finite amplitude types are typically Korteweg-de Vries (kdV) solitons, while the arbitrary amplitude is generally studied by using the Sagdeev pseudo-potential technique. Earlier theoretical studies have considered either Maxwell or nonthermal (kappa or Cairns type) particle distributions to study electron [35–50] and ion-acoustic [51–56] solitons in space plasmas. Mamun and Shukla [57] studied the nonlinear propagation of finite and arbitrary amplitude electron-acoustic solitary waves in an auroral plasma composed of established two electron species composed of cold electron fluid and hot trapped distribution electron, and stationary ions. In addition, theoretical interpretation of ESWs observed by the Van Allen Probes mission in the Earth's inner magnetosphere has been done [32,58], using the fluid dynamics approach to derive the modified Korteweg-de Vries (KdV) equation of waves for the existence of nonlinear, collisionless electron-acoustic solitons and double layers (shock waves). Shock wave solutions normally arise due to the plasma particles collisions. In the presence of wave dissipation (shock) due to particles collision (viscosity), the dynamics of the nonlinear wave are governed by the KdV-Burgers equation, where the Burgers term account for the shock structures. This is caused by the balance between the nonlinearity and the merged force of dispersion and dissipation. However, the generation mechanism of ESWs in the EDR observed by MMS mission still lacks in theory.

In this paper, we study the small but finite amplitude nonlinear electron-acoustic waves in the EDR. The plasma model consists of hot magnetospheric electrons having a trapped or vortex-like kinetic velocity distribution, adiabatic warm magnetosheath electron fluid and background stationary ions. This is an extension of the work of Mamun and Shukla [57] where we have included finite cold electron temperature which was neglected in their model. This is done in keeping view of the observations in the EDR. The present model is capable of explaining the MMS ESWs with asymmetric bipolar parallel electric field structures using a hybrid of a kinetic velocity distribution and fluid dynamic equations, resulting in the formation of nonlinear solitons. Further, for the sake of completeness, viscosity term has been incorporated, though not applicable in space plasmas but can be useful in the lower atmosphere. The space plasma model is presented and solved using the reductive perturbation technique to obtain the KdV-like equations in Section "Theoretical model". The analytical solutions of the derived modified KdV equation are presented in Section "Nonlinear wave solutions". Numerical results are discussed in Section "Numerical results". The conclusions are presented in Section "Conclusion".

Theoretical model

The EDR plasma model adopted in this study is based on observations from the MMS mission [9,20]. Our plasma model consists of two electron populations of a hot ($\sim$ 1 keV) magnetospheric electrons having a kinetic vortex-like velocity distribution[61], magnetosheath warm ($\sim$ 100 eV) electrons and background stationary ions [9]. Due to the large ion to electron mass ratio, ions do not contribute significantly to high frequency waves, hence, their dynamics is neglected [33,59]. We have also included viscosity in our model. The dynamics of warm election species can be described by fluid continuity and momentum equations in normalized form,

$$\frac{\partial n_w}{\partial t}+\frac{\partial}{\partial z}(n_w v_w)=0 \tag{1}$$

$$\frac{\partial v_w}{\partial t}+v_w\frac{\partial v_w}{\partial z}=\frac{\partial \phi}{\partial z}-\frac{\gamma\sigma_w}{n_w}\frac{\partial n_w}{\partial z}+\eta\frac{\partial^2 v_w}{\partial z^2} \tag{2}$$

where n_w, v_w, m_e are the warm electron number density, fluid velocity and mass of the electrons, e is the magnitude of the electron charge, ϕ is electrostatic potential, the temperature $\sigma_w = \frac{T_w}{T_h}$, where $T_w(T_h)$ is the warm (hot) temperature, η is the normalized viscosity due to collisions and $\gamma = 3$ for adiabatic plasma temperature [32].

Assuming that the hot electrons trapping in the holes along the line of force of the external magnetic field and develop the vortex-like velocity distribution function given by Schamel[60,61],

$$n_h = I(\phi)+|\beta|^{-1/2}\begin{cases}\exp(\beta\phi)\mathrm{erf}(\sqrt{\beta\phi}) & \beta\geqslant 0\\ \frac{2}{\sqrt{\pi}}W_D(\sqrt{-\beta\phi}) & \beta<0\end{cases} \tag{3}$$

where

$$I(x)=(1-\mathrm{erf}(\sqrt{x}))\exp(x),\quad W_D(x)=\exp(-x^2)\int_0^x\exp(y^2)dy,$$

where $\mathrm{erf}(x)$ is the error function and β controls the trapping of electrons and sharp of the distribution function. The Maxwell–Boltzmann equilibrium of hot electron can be recovered in the limit $\beta\to 1$ ($\beta\to 0$). For $\phi\ll 1$, the normalized hot trapped electron density can be expressed as

$$n_h = n_{h0}\left(1+\phi-\frac{4(1-\beta)}{3\sqrt{\pi}}\phi^{3/2}+\frac{\phi^2}{2}+\ldots.\right) \tag{4}$$

For high frequency waves, the system of equations can be closed with the Poisson equation

$$-\frac{\partial^2\phi}{\partial z^2}=1-n_w-n_h. \tag{5}$$

Eqs. (1)–(5) are a normalized set of equations. The densities are normalized by the total equilibrium density $N_0 = N_{w0} + N_{h0}$, where $N_{h0}/N_0 = n_{h0}$ and $N_{w0}/N_0 = n_{w0}$. Velocities are normalized by the thermal velocity of hot electrons $v_{th} = \sqrt{T_h/m_e}$, lengths by the effective hot electron Debye length $\lambda_d = \sqrt{T_h/4\pi N_0 e^2}$, temperature by the hot trapped electron temperature T_h, time by the inverse of the electron plasma frequency $\omega_{p0}^{-1} = \sqrt{m_e/4\pi N_0 e^2}$, the electrostatic potential ϕ is normalized by T_h/e, respectively. Here 'e' and m_e are the charge and mass of the electrons, respectively. The phase velocity of the nonlinear

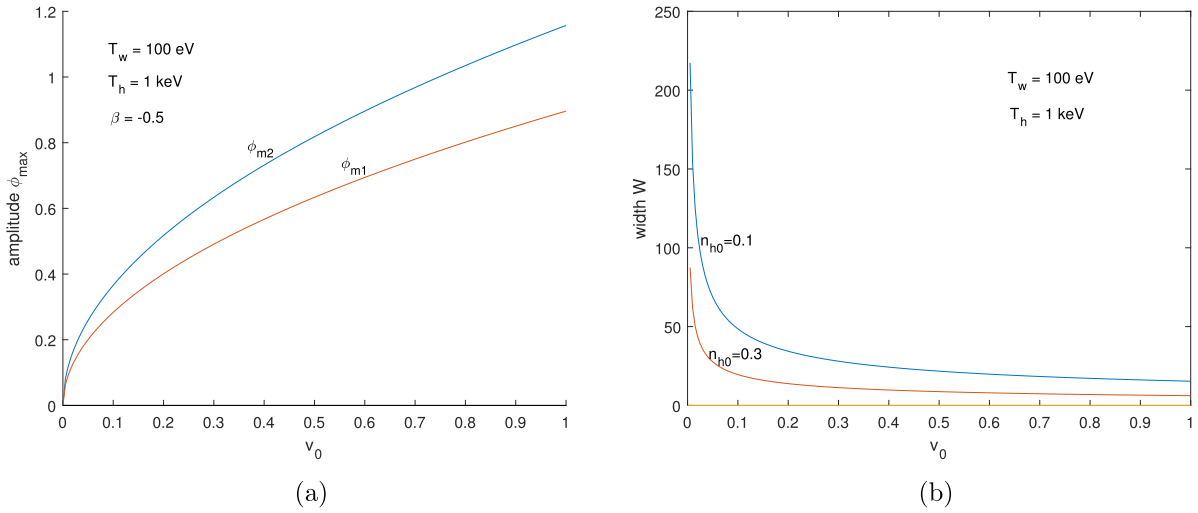

Fig. 2. (a) Electrostatic wave amplitude profiles ϕ vs v_0 for $\beta = -0.5$, (b) Soliton width profiles W vs v_0.

electron-acoustic waves is greater than electron-acoustic velocity, $v_s = v_{th}(N_{w0}/N_{h0})^{1/2}$.

The linear dispersion relation of electron-acoustic waves (for $\eta \to 0$) can be obtained from the set of Eqs. (1), (2), (4) and (5) and can be written as

$$1 + \frac{1}{k^2\lambda_{dh}^2} - \frac{\omega_{pw}^2}{\omega^2 - \gamma k^2 v_{tw}^2} = 0. \tag{6}$$

where $v_{tw} = \sqrt{T_w/m_e}$ is the thermal speed of the warm electrons, and T_w and m_j are the equilibrium temperature and mass of the jth species, respectively and $\lambda_{dh} = \sqrt{T_h/4\pi N_{h0}e^2}$ is the hot electron Debye length.

Then, with the help of an infinitesimal parameter ϵ, reductive perturbation analysis will be performed for the existence of nonlinear KdV-like equation of the localized shock and soliton solutions. The analysis involved the construction of stretched coordinates,

$$\xi = \epsilon^{1/4}(z - Mt), \quad \tau = \epsilon^{3/4}t \tag{7}$$

where M is the phase velocity of the electrostatic structures normalized by the hot electron thermal speed v_{th} and ϵ is a dimensionless parameter that measures the order of smallness and $\eta = \epsilon^{1/4}\eta_0$. The dependent variables n, v and ϕ are perturbed in a power series of the dispersive terms ϵ around their equilibrium

$$\begin{pmatrix} n_w \\ v_w \\ \phi \\ n_h \end{pmatrix} = \begin{pmatrix} n_{w0} \\ 0 \\ 0 \\ n_{h0} \end{pmatrix} + \begin{pmatrix} \epsilon n_{w1} + \epsilon^{3/2} n_{w2} + \ldots.. \\ \epsilon v_{w1} + \epsilon^{3/2} v_{w2} + \ldots... \\ \epsilon\phi_1 + \epsilon^{3/2}\phi_2 + ... \\ \epsilon n_{h1} + \epsilon^{3/2} n_{h2} + \ldots.. \end{pmatrix}. \tag{8}$$

Using Eqs. (7) and (8), the set of Eqs. (1), (2), (4) and (5) can be reduced to the form of a modified KdV-Burgers equation

$$\frac{\partial\phi_1}{\partial\tau} + A\phi_1^{\frac{1}{2}}\frac{\partial\phi_1}{\partial\xi} - C\frac{\partial^2\phi_1}{\partial\xi^2} + B\frac{\partial^3\phi_1}{\partial\xi^3} = 0, \tag{9}$$

for the phase velocity $M \approx (\frac{n_{w0}}{n_{h0}} + 3\sigma_w)^{1/2}$, where A is the nonlinearity coefficients, B is the dispersion coefficient and C is the dissipation term

$$\begin{cases} A = & \dfrac{(M^2 - 3\sigma_w)(1-\beta)}{M\sqrt{\pi}}, \\ B = & \dfrac{M^2 - 3\sigma_w}{2Mn_{h0}}, \\ C = & \dfrac{\eta_0}{2}. \end{cases} \tag{10}$$

This evolution equation is known as the modified KdV-Burgers or trapped KdV-Burgers equation.

In a collisionless plasma, i.e. in the limit viscosity tends to be zero ($\eta = 0$). The momentum equation in (2) will be reduced to that of Eq. (2) of Dillard et al. [32]. Then, through the same algebraic system above, one is expected to get a KdV-like equation with the nonlinearity coefficients A and dispersion coefficient B of the form,

$$\frac{\partial\phi_1}{\partial\tau} + A\phi_1^{\frac{1}{2}}\frac{\partial\phi_1}{\partial\xi} + B\frac{\partial^3\phi_1}{\partial\xi^3} = 0 \tag{11}$$

Eq. (11) is a modified KdV or trapped KdV equation.

Nonlinear wave solutions

A stationary wave solution of the nonlinear modified KdV (mKdV) Eq. (11) can be obtained by transforming the space variable into traveling wave [62] frame $\chi = \kappa(\xi - v_0\tau)$, where κ and v_0 are related to the inverse width and wave speed respectively, and both are assumed to be positive. Then, the system will be in the form of $\phi_1(\xi,\tau) = u(\chi)$ and the mKdV (11) reduces to

$$-v_0\frac{du}{d\chi} + Au^{\frac{1}{2}}\frac{du}{d\chi} + Bk^2\frac{d^3u}{d\chi^3} = 0. \tag{12}$$

Using the hyperbolic tangent (Tanh) method of Malfliet and Hereman [62], and Kourakis et al. [67], it is certain that a wave solution will be obtained due to the dispersion term. Now, let $u(\chi) = w^2(\chi)$ (to relieve the power of $\frac{1}{2}$ in the nonlinear term), where $w(\chi) = S(\tanh\chi) = S(y)$. Eq. (12) becomes

$$-v_0\frac{w^2}{2} + A\frac{w^3}{3} + Bk^2\left[\left(\frac{dw}{d\chi}\right)^2 + w\frac{d^2w}{d\chi^2}\right] = 0 \tag{13}$$

Eq. (13) has a power series solution of the form $S(y) = a_0 + a_1y + a_2y^2$, due to the balancing between the highest nonlinearity and dispersive terms. Then, the general solution of the Eq. (11) can be written as

$$u(\chi) = w^2(\chi) = (a_0 + a_1\tanh\chi + a_2\tanh^2\chi)^2 \tag{14}$$

where

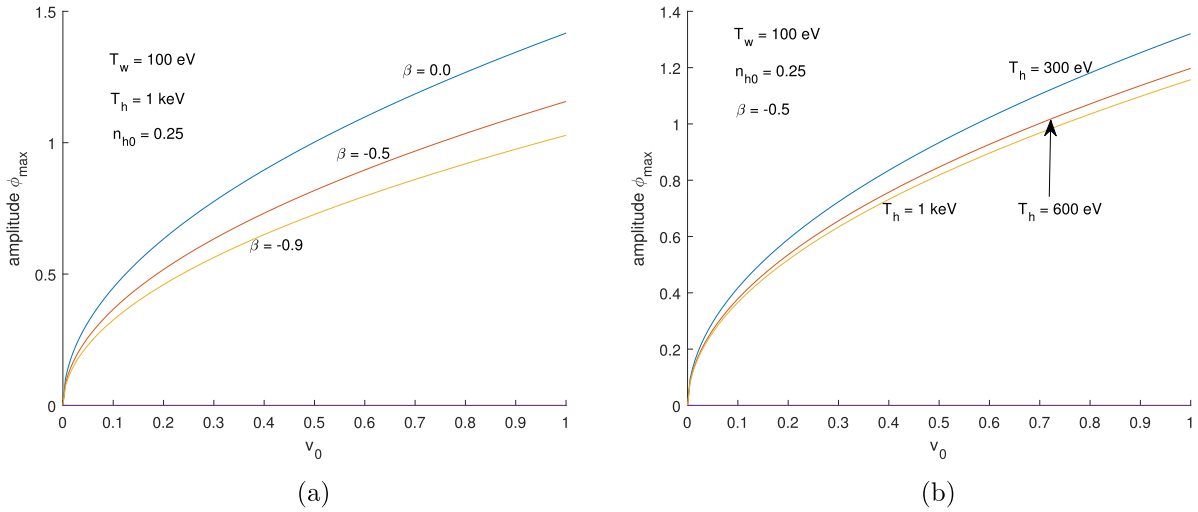

Fig. 3. Electrostatic wave amplitude profiles ϕ vs v_0 for β (a) and T_h(b) for $n_{h0} = 0.25$.

$$a_0 = \frac{18Bk^2}{A} = -a_2, \quad a_1 = 0, \quad \text{or} \quad a_0 = \frac{30Bk^2}{A} = -a_2, \quad a_1 = 0, \quad k = \sqrt{\frac{v_0}{16B}}. \tag{15}$$

Therefore, Eq. (14) can be written as

$$\phi_1(\xi,\tau) = [a_0 + a_2 \tanh^2\{k(\xi - v_0\tau)\}]^2 \tag{16}$$

Using the values of the coefficients a_0 and a_2 in Eq. (16), the solution can be written as

$$\phi_1(\xi,\tau) = \phi_{max}\text{sech}^4\left(\frac{\xi - v_0\tau}{W}\right). \tag{17}$$

From Eq. (17), it is obvious that electron acoustic solitons can have only positive amplitude with maximum amplitude being $\phi_{max} = (9v_0/8A)^{1/2} = \phi_{m1}$ or $(15v_0/8A)^{1/2} = \phi_{m2}$ and the soliton width $W(= k^{-1}) = 4\sqrt{B/v_0}$. The amplitude of the soliton will be $\phi = \epsilon\phi_1$ (refer to Eqn. (8))

Numerical results

The characteristics of nonlinear electron-acoustic waves in an unmagnetized EDR plasma can be investigated numerically by computing the analytical solution of the modified KdV equations using the MMS data recorded by Ergun et al. [9]. The parameters are as follows [9]: the hot magnetospheric electron temperature and density, $T_h = 1$ keV and $N_{h0} = 0.5\ cm^{-3}$, warm magnetosheath electron temperature and density, $T_w = 100$ eV and $N_{w0} = 1.5\ cm^{-3}$. For the selected plasma parameters, the electron-acoustic wave speed is found within the supersonic region.

In Fig. 2 (a), the maximum amplitude ϕ_{max} against the wave speed (v_0) are plotted for $\beta = -0.5$. Fig. 2 (b) shows the variation of soliton width vs v_0 for different values of n_{h0}. The soliton width decreases with hot electron number density (n_{h0}).

The electrostatic potential amplitude profiles in Fig. 3 shows the variation of β (a) and hot electron temperature T_h for $n_{h0} = 0.25$. The curve $\beta = 0$ corresponds to the Boltzmann hot electron distribution provides a standard KdV equation [63] solution, whereas the vortex hot electron distribution of negative β-values exhibit strong nonlinearity of mKdV Eq. (11), corresponding to smaller amplitude. Fig. 3 (b) shows that the electrostatic wave amplitude decreases with increase in hot electron temperature T_h.

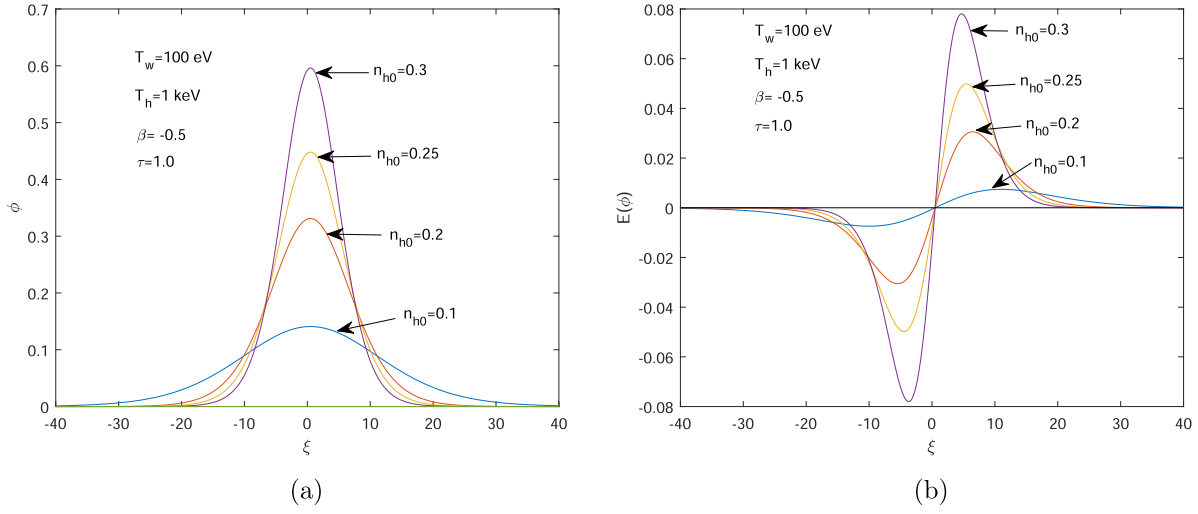

Fig. 4. (a) Soliton profiles ϕ vs ξ for $v_0 = 0.5$, (b) corresponding bipolar electric field profiles of the solitons.

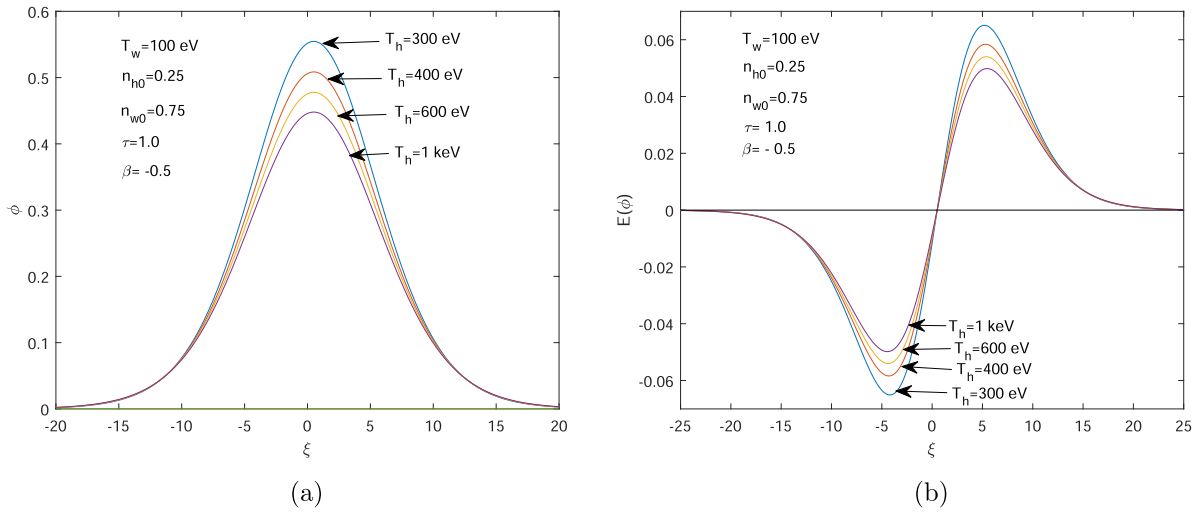

Fig. 5. (a) Soliton profiles ϕ vs ξ for $v_0 = 0.5$, (b) corresponding bipolar electric field profiles of the solitons.

Fig. 4 shows the electron-acoustic soliton profiles, i.e., normalized electrostatic potential ϕ vs time ξ for different values of hot electron number density n_{h0} for $\beta = -0.5$. The other fixed plasma parameters are $T_w = 100$ eV, $T_h = 1$ keV, time $\tau = 1.0$, and $v_0 = 0.5$. It is observed that as the hot electron density increases, the electron-acoustic soliton amplitude increases and its width decreases. The corresponding bipolar electric field profiles are in Fig. 4 (b).

Fig. 5 shows the electron-acoustic soliton potential profiles of modified KdV equation for different values of hot electron temperature T_h, for hot electron number density $N_{h0}/N_0 = n_{h0} = 0.25$, warm electron number density $N_{w0}/N_0 = n_{w0} = 0.75$ and other fixed plasma parameters are as in Fig. 4. The corresponding bipolar electric field profiles are in Fig. 5 (b). The electron-acoustic wave amplitude decreases with increase in hot electron temperature T_h, which corresponds to the Fig. 3 (b) above. It is noticed that as soliton amplitude increases its width also increases. This trend of soliton width increasing with increasing amplitude has also been observed in POLAR observations of ion and electron mode solitary waves [64,65] and theoretically [66].

Conclusion

Finite amplitude nonlinear electron-acoustic waves in the electron diffusion region have been studied in a plasma consisting of hot magnetospheric trapped electrons, warm magnetosheath electrons and background stationary ions. The model support the existence of positive potential finite amplitude electron-acoustic solitons propagating with supersonic speed above the electron sound speed. Thermal effect of adiabatic electron fluid are taken into account which were neglected for the case of an auroral plasma [57]. It is found that as the value of the hot electron temperature increases, the electric field amplitude decreases. It is also observed that the electron-acoustic soliton amplitude increases with number density but decreases with the hot electron temperature. However, soliton amplitude as well as width increases in the case of hot electron temperature variation whereas it shows the usual behavior of soliton amplitude increasing and width decreasing for the case of hot electron density variation.

The observations from the MMS missions at the Earth's magnetopause [9] revealed nonlinear electrostatic solitary structures with electric field amplitude varies from ~ 1 mV/m up to ~ 100 mV/m. For the typical MMS parameters [9], namely, $T_h = 1$ keV, $T_w = 100$ eV, $N_0 = 2$ cm^{-3}, the typical electric field associated with soliton for $\tau = 1.0, v_0 = 0.5$, and $\beta = -0.5$ are found to be ≈ 30 mV/m, the corresponding soliton width, pulse duration, and speed comes out to be ≈ 2291 m, $\approx 95\mu s$, and 2.4×10^4 km/s, respectively. The results obtained here may be helpful in explaining the characteristics of the nonlinear electrostatic fluctuations observed by the Magnetospheric Multiscale Mission (MMS).

CRediT authorship contribution statement

Odutayo R. Rufai: Conceptualization, Methodology, Writing - original draft, Formal analysis, Visualization. **George V. Khazanov:** Supervision. **S.V. Singh:** Validation, Writing - review & editing.

Declaration of Competing Interest

The authors declare that they have no known competing financial interests or personal relationships that could have appeared to influence the work reported in this paper.

Acknowledgments

ORR would like to acknowledge the financial support of the NASA/USRA Postdoctoral Fellowship Program (NPFP). Data is available through [9]. MMS data are also open to the public.

Appendix A

Using the hyperbolic tangent (Tanh) method, the modified KdV-Burgers Eq. (9) can be written as

$$-v_0\frac{w^2}{2}+A\frac{w^3}{3}+Bk^2\left[\left(\frac{dw}{d\chi}\right)^2+w\frac{d^2w}{d\chi^2}\right]-Ck\left[w\frac{dw}{d\chi}\right]=0, \tag{18}$$

the general solution becomes

$$u(\chi) = (a_0 + a_1 \tanh\chi + a_2 \tanh^2\chi)^2, \tag{19}$$

where

$$a_0 = \frac{5v_0}{8A} + \frac{20Bk^2}{A}, \quad a_1 = \frac{-10Ck}{3A}, \quad a_2 = \frac{-30Bk^2}{A}, \tag{20}$$

and possible values for v_0 and k are

$$v_0 = 32Bk^2, \quad k = \frac{C}{3B\sqrt{6}}. \tag{21}$$

References

[1] Escoubet CP, Fehringer M, Goldstein M. The cluster mission. Ann Geophys 2001; 19:1197–200. https://doi.org/10.5194/angeo-19-1197-2001.

[2] Graham DB, Khotyaintsev YuV, Vaivads A, Andre M. Electrostatic solitary waves with distinct speeds associated with asymmetric reconnection. Geophys Res Lett 2015;42:215224.

[3] Angelopoulos V. The THEMIS mission. Space Sci Rev 2008;141:5. https://doi.org/10.1007/s11214-008-9336-1.

[4] Wang C-P, Gkioulidou M, Lyons LR, Angelopoulos V. Spatial distributions of the ion to electron temperature ratio in the magnetosheath and plasma sheet. J Geophys Res 2012;117:A08215. https://doi.org/10.1029/2012JA017658.

[5] Burch JL, Torbert RB, Phan TD, Chen L-J, Moore TE, Ergun RE, Eastwood JP, Gershman DJ, Cassak PA, Argall MR, Wang S, Hesse M, Pollock CJ, Giles BL, Nakamura R, Mauk BH, Fuselier SA, Russell CT, et al. Electron-scale measurements of magnetic reconnection in space. Science 2016;352:6290. https://doi.org/10.1126/science.aaf2939.

[6] Viberg H, Khotyaintsev YV, Vaivads A, Andre M, Pickett JS. Mapping HF waves in the reconnection diffusion region. Geophys Res Lett 2013;40:1032–7. https://doi.org/10.1002/grl.50227.

[7] Osman KT, Kiyani K, Matthaeus WH, Hnat B, Chapman SC, Khotyaintsev YV. Multi-spacecraft measurment of turbulence within a magnetic reconnection jet. Astrophys J 2015;815(L24). https://doi.org/10.1088/2041-8205/815/2/L24.

[8] Fu HS, Vaivads A, Khotyaintsev YV, Andre M, Cao JB, Olshevsky V, et al. Intermittent energy dissipation by turbulent reconnection. Geophys Res Lett 2017; 44:37–43. https://doi.org/10.1002/2016GL071787.

[9] Ergun RE, Holmes JC, Goodrich KA, Wilder FD, Stawarz JE, Eriksson S, Newman DL, Schwartz SJ, Goldman MV, Sturner AP, Malaspina DM, Usanova ME, Torbert RB, Argall M, et al. Magnetospheric Multiscale observations of large-amplitude, parallel, electrostatic waves associated with magnetic reconnection at the magnetopause. Geophys Res Lett 2016;43:5626–34. https://doi.org/10.1002/2016GL068992.

[10] Zhou M, Ashour-Abdalla M, Berchem J, Walker RJ, Liang H, El-Alaoui M, Goldstein ML, Lindqvist P-A, Marklund G, Khotyaintsev YV, Ergun RE, et al. Observation of high-frequency electrostatic waves in the vicinity of the reconnection ion diffusion region by the spacecraft of the Magnetospheric Multiscale (MMS) mission. Geophys Res Lett 2016;43:4808–15. https://doi.org/10.1002/2016GL069010.

[11] Argall MR, Paulson K, Alm L, Rager A, Dorelli J, Shuster J, Wang S, Torbert RB, Vaith H, Dors I, Chutter M, Farrugia C, Burch J, Pollock C, Giles B, et al. Electron dynamics within the electron diffusion region of asymmetric reconnection. J Geophys Res: Space Phys 2018;123:146–62. https://doi.org/10.1002/2017JA024524.

[12] Yamada M, Chen L-J, Yoo J, Wang S, Fox W, jara-Almonte J, et al. The two-fluid dynamics and energetics of the asymmetric magnetic reconnection in laboratory and space plasmas. Nature Commun 2018;9:5223. https://doi.org/10.1038/s41467018-07680-2.

[13] Peng FZ, Fu HS, Cao JB, Graham DB, Chen ZZ, Cao D, Xu Y, Huang SY, Wang TY, Khotyaintsev YV, Andre M, Russell CT, Giles B, Lindqvist P-A, Torbert RB, Ergun RE, Burch JL. Quadrupolar pattern of the asymmetric guide-field reconnection. J Geophys Res Space Phys 2017;122:6349–56. https://doi.org/10.1002/2016JA023666.

[14] Fu HS, Peng FZ, Liu CM, Burch JL, Gershman DG, et al. Evidence of Electron Acceleration at a Reconnecting Magnetopause. Geophys Res Lett 2019;46(11): 5645–52. https://doi.org/10.1029/2019GL083032.

[15] Chen L-J, Wang S, Hesse M, Ergun RE, Moore T, Giles B, Bessho N, Russell C, Burch J, Torbert RB, Genestreti KJ, Paterson W, Pollock C, Lavraud B, Le Cantel O, Strangeway R, Khotyaintsev YuV, Lindqvist P-A. Electron diffusion regions in magnetotail reconnection under varying guide fields. Geophys Res Lett 2019;46: 6230–8. https://doi.org/10.1029/2019GL082393.

[16] Hwang K-J, Choi E, Dokgo K, Burch JL, Sibeck DG, Giles BL, Goldstein ML, Paterson WR, Pollock CJ, Shi QQ, Fu H, Hasegawa H, Gershman DJ, Khotyaintsev Y, Torbert RB, Ergun RE, Dorelli JC, Avanov L, Russell CT, Strangeway RJ. Electron vorticity indicative of the electron diffusion region of magnetic reconnection. Geophys Res Lett 2019;46:6287–96. https://doi.org/10.1029/2019GL082710.

[17] Torbert RB, Burch JL, Phan TD, Hesse M, Argall MR, Shuster J, Ergun RE, Alm L, Nakamura R, Gershman KJ, Paterson WR, Turner DL, Cohen I, Giles BL, Pollock CJ, et al. Electron-scale dynamics of the diffusion region during symmetric magnetic reconnection in space. Science 2018;362:1391–5. https://science.sciencemag.org/content/sci/362/6421/1391.full.pdf.

[18] Nakamura R, Genestreti KJ, Nakamura T, Baumjohann W, Varsani A, Nagai T, et al. Structure of the current sheet in the 11 July 2017 electron diffusion region event. J Geophys Res: Space Physics 2019;124:1173–86. https://doi.org/10.1029/2018JA025713.

[19] Wang Z, Fu HS, Liu CM, Liu YY, Cozzani G, Giles BL, Hwang K-J. J.L. Burch, Electron distribution functions around a reconnection X-line resolved by the FOTE method. Geophys Res Lett 2019;46:1195–204. https://doi.org/10.1029/2018GL081708.

[20] Bessho N, Chen L-J, Hesse M. Electron distribution functions in the diffusion region of asymmetric magnetic reconnection. Geophys Res Lett 2016;43:1828–36. https://doi.org/10.1002/2016GL067886.

[21] Egedal J, Le A, Daughton W, Wetherton B, Cassak PA, Chen L-J, Avanov LA. Spacecraft observations and analytic theory of crescent-shaped electron distributions in asymmetric magnetic reconnection. Phys Rev Lett 2016;116(23): 235102. https://doi.org/10.1103/PhysRevLett.117.185101.

[22] Hesse M, Liu Y-H, Chen L-J, Bessho N, Kuznetsova M, Birn J, Burch JL. On the electron diffusion region in asymmetric reconnection with a guide magnetic field. Geophys Res Lett 2016;43:2359–64. https://doi.org/10.1002/2016GL068373.

[23] Nakamura TKM, Eriksson S, Hasegawa H, Zenitani S, Li W, Genestreti KJ, et al. Mass and energy transfer across the Earth's magnetopause caused by vortex-induced reconnection. J Geophys Res: Space Phys 2017;122. https://doi.org/10.1004/2017JA024346. 11,505–11, 522.

[24] Khotyaintsev YV, Graham DB, Norgren C, Vaivads A. Collisionless Magnetic Reconnection and Waves: Progress Review. Front Astron Space Sci 2019;6:70. https://doi.org/10.3389/fspas.2019.00070.

[25] Graham DB, Vaivads A, Khotyaintsev YuV, Andre M, Le Contel O, Malaspina DM, Lindqvist P-A, Ergun RE, Gershman DJ, Giles BL, Magnes W, Russell CT, Burch JL, Torbert RB. Large-amplitude high-frequency waves at Earth's magnetopause. J Geophys Res: Space Phys 2018;123:2630–57. https://doi.org/10.1002/2017JA025034.

[26] Mozer FS, Agapitov OV, Giles B, Vasko I. Direct observations of electron distributions inside millisecond duration electron holes. Phys Rev Lett 2018;121: 135102. https://doi.org/10.1103/PhysRevLett.121.135102.

[27] Fu HS, Chen F, Chen ZZ, Xu Y, Wang Z, Liu YY, Liu CM, Khotyaintsev YV, Ergun RE, Giles BL, Burch JL. First measurements of electrons and waves inside an electrostatic solitary wave. Phys Rev Lett 2020;124:095101. https://doi.org/10.1103/PhysRevLett.124.095101.

[28] Mozer FS, Agapitov OV, Artemyev A, Drake JF, Krasnoselskikh V, Lejosne S, Vasko I. Time domain structures: What and where they are, what they do, and how they are made. Geophys Res Lett 2015;42:3627–38. https://doi.org/10.1002/2015GL063946.

[29] Lakhina GS, Singh SV, Kakad AP, Goldstein ML, Vinas AF, Pickett JS. A mechanism for electrostatic solitary structures in the Earth's magnetosheath. J Geophys Res 2009;114:A09212. https://doi.org/10.1029/2009JA014306.

[30] Hutchinson IH. Electron holes in phase space: What they are and why they matter. Phys Plasmas 2017;24(5):055601. https://aip.scitation.org/doi/10.1063/1.4976854.

[31] Vasko IY, Agapitov OV, Mozer FS, Bonnell JW, Artemyev AV, Krasnoselskikh VV, Tong Y. Phys Rev Lett 2018;120:195101.

[32] Dillard CS, Vasko IY, Mozer FS, Agapitor OV, Bonnell JW. Electron-acoustic solitary waves in the Earth inner magnetosphere. Phys Plasmas 2018;25:022905. https://doi.org/10.1063/1.5007907.

[33] Lotekar A, Kakad A, Kakad B. Formation of Asymmetric electron acoustic double layers in the Earth's inner magnetosphere. J Geophys Res: Space Phys 2019;124: 6896–905. https://doi.org/10.1029/2018JA026303.

[34] Gary SP, Tokar RL. The electron-acoustic mode. Phys Fluids 1985;28:2439–41. https://doi.org/10.1063/1.865250.

[35] Rubia R, Singh SV, Lakhina GS. Existence domain of electrostatic solitary waves in the lunar wake. Phys Plasmas 2018;25(3):032302. https://doi.org/10.1063/1.5017638.

[36] Singh SV, Lakhina GS. Generation of electron-acoustic waves in the magnetosphere. Planet Space Sci 2001;49(1):107–14.

[37] Singh SV, Reddy RV, Lakhina GS. Broadband electrostatic noise due to nonlinear electron-acoustic waves. Adv Space Res 2001;28(11):1643–8.

[38] Singh SV, Lakhina GS. Electron acoustic solitary waves with non-thermal distribution of electrons. Nonln Processes Geophys 2004;11:275–9. doi:10.5194/npg-11-275-2004.
[39] Singh SV, Lakhina GS, Bharuthram R, Pillay SR. Electrostatic solitary structures in presence of non-thermal electrons and a warm electron beam on the auroral field lines. Phys Plasmas 2011;18:122306. https://doi.org/10.1063/1.3671955.
[40] Singh SV, Devanandhan S, Lakhina GS, Bharuthram R. Electron acoustic solitary waves in a magnetized plasma with nonthermal electrons and an electron beam. Phys Plasmas 2016;23(8):082310. https://doi.org/10.1063/1.4961961.
[41] Mbuli LN, Maharaj SK, Bharuthram R, Singh SV, Lakhina GS. Arbitrary amplitude fast electron-acoustic solitons in three-electron component space plasmas. Phys Plasmas 2016;23(6):062302. https://doi.org/10.1063/1.4952637.
[42] Mbuli LN, Maharaj SK, Bharuthram R, Singh SV, Lakhina GS. Arbitrary amplitude slow electron-acoustic and ion-acoustic solitons in three-electron temperature space plasmas. Phys Plasmas 2015;22:062307. https://doi.org/10.1063/1.4922683.
[43] Devanandhan S, Singh SV, Lakhina GS, Bharuthram R. Electron-acoustic solitons in the presence of an electron beam and superthermal electrons. Nonln Processes Geophys 2011;18:627–34. https://doi.org/10.5194/npg-18-627-2011.
[44] Devanandhan S, Singh SV, Lakhina GS. Electron acoustic solitary waves with kappa-distributed electrons. Phys Scr 2011;84:025507. https://doi.org/10.1088/0031-8949/84/02/025507.
[45] Devanandhan S, Singh SV, Lakhina GS, Bharuthram R. Electron acoustic waves in a magnetized plasma with kappa distributed ions. Phys Plasmas 2012;19:082314. https://doi.org/10.1063/1.4743015.
[46] Devanandhan S, Singh SV, Lakhina GS, Bharuthram R. Small amplitude electron acoustic solitary waves in a magnetized superthermal plasma. Commun Nonlinear Sci Numer Simul 2015;22(1–3):1322–30. https://doi.org/10.1016/j.cnsns.2014.07.026.
[47] Maharaj SK, Bharuthram R, Singh SV. G.S. Lakhina Existence domains of arbitrary amplitude nonlinear structures in two-electron temperature space plasmas: II. High-frequency electron-acoustic solitons. Phys Plasmas 2012;19:122301. https://doi.org/10.1063/1.4769174.
[48] Lakhina GS, Singh SV, Kakad AP. Ion- and electron-acoustic solitons and double layers in multi-component space plasmas. Adv Space Res 2011;47:1558–67. https://doi.org/10.1016/j.asr.2010.12.013.
[49] Pickett JS, Chen L-J, Mutel RL, Christopher IH, Santolik O, Lakhina GS, Singh SV, Reddy RV, Gurnett DA, Tsurutani BT, Lucek E. Furthering our understanding of electrostatic solitary waves through Cluster multi-spacecraft observations and theory. Adv Space Res 2008;41:1666–76.
[50] Tagare SG, Singh SV, Reddy RV, Lakhina GS. Electron-acoustic solitons in the Earth's magnetotail. Nonln Processes Geophys 2004;11:215–8.
[51] Rufai OR, Bharuthram R, Singh SV, Lakhina GS. Low frequency solitons and double layers in a magnetized plasma with two temperature electrons. Phys Plasmas 2012;19:122308.
[52] Rufai OR, Bharuthram R, Singh SV, Lakhina GS. Effect of hot ion temperature on obliquely propagating ion-acoustic solitons and doubles in an auroral plasma. Commun Nonlin Sci Numer Simul 2014;19:1338–46.
[53] Rufai OR, Bharuthram R, Singh SV, Lakhina GS. Ion acoustic solitons and supersolitons in a magnetized plasma with nonthermal hot electrons and Boltzmann cool electrons. Phys Plasmas 2014;21:082304.
[54] Rufai OR, Bharuthram R, Singh SV, Lakhina GS. Effect of excess superthermal hot electrons on finite amplitude ion-acoustic solitons and supersolitons in a magnetized auroral plasma. Phys Plasmas 2015;22:102305.
[55] Rufai OR, Bharuthram R. Obliquely propagating low-frequency magnetospheric electrostatic solitary waves in the presence of an oxygen-ion beam. Commun Nonlin Sci Numer Simul 2019;68:160.
[56] Rufai OR. Periodic low-frequency electric field structures in a magnetized nonthermal auroral plasma. HELIYON 2019;5, 7:e01976.
[57] Mamun AA, Shukla PK. Electron-acoustic solitary waves via vortex electron distribution. J Geophys Res 2002;107, A7:1135. https://doi.org/10.1029/2001JA009131.
[58] Vasko IY, Agapitov OV, Mozer FS, Bonnell JW, Artemyev AV, Krasnoselskikh VV, Reeves G, Hospodarsky G. Electron-acoustic solitons and double-layers in the inner magnetosphere. Geophys Res Lett 2017;44:4575–83. https://doi.org/10.1002/2017GL074026.
[59] Watanabe K, Taniuti T. Electron-acoustic mode in a plasma of two-temperature electrons. J Phys Soc Jpn 1977;43:1819. https://doi.org/10.1143/JPSJ.43.1819.
[60] Schamel H. Stationary solitary, snoidal and sinusoidal ion acoustic waves. Plasma Phys 1972;14:905. https://iopscience.iop.org/article/10.1088/0032-1028/14/10/002.
[61] Schamel H. Theory of electron holes. Physica Scripta 1979;20:336–42.
[62] Malfliet W, Hereman W. The Tanh method: I. Exact solutions of nonlinear evolution and wave equations. Phys Scr 1996;54:563–8.
[63] Mace RL, Baboolal S, Bharuthram R, Hellberg MA. Arbitary-amplitude electron-acoustic solitons in a two-electron-component plasma. J Plasma Phys 1991;45(3):323–38.
[64] Dombeck J, Cattell C, Crumley J, Peterson WK, Collin HL, Kletzing C. Observed trends in auroral zone ion mode solitary wave structure characteristics using data from Polar. J Geophys Res 2001;106:19 013–19 021.
[65] Cattell CA, Crumley J, Dombeck J, Lysak R, Kletzing C, Peterson WK, Collin C. Polar observations of solitary waves at high and low altitudes and comparison to theory. Adv Space Res 2001;28:1631–41.
[66] Ghosh SS, Lakhina GS. Anomalous width variation of rarefactive ion acoustic solitary waves in the context of auroral plasmas. Nonlinear Processes Geophys 2004;11:219–28.
[67] Kourakis I, Sultana S, Verheest F. Note on the single-shock solutions of the Korteweg-de Vries-Burgers equation. Astrophys Space Sci 2012;338:245.